Soft Matter

PAPER

View Article Online
View Journal | View Issue

Cite this: *Soft Matter*, 2014, **10**, 3016

Inter-particle correlations in a hard-sphere colloidal suspension with polymer additives investigated by Spin Echo Small Angle Neutron Scattering (SESANS)

A. L. Washington,*[a] X. Li,[ab] A. B. Schofield,[c] K. Hong,[d] M. R. Fitzsimmons,[e] R. Dalgliesh[f] and R. Pynn[ab]

Received 3rd December 2013
Accepted 10th February 2014

DOI: 10.1039/c3sm53027b

www.rsc.org/softmatter

Using a neutron scattering technique that measures a statistically-averaged density correlation function in real space rather than the conventional reciprocal-space structure factor, we have measured correlations between poly(methyl-methacrylate) (PMMA) colloidal particles of several sizes suspended in decalin. The new method, called Spin Echo Small Angle Neutron Scattering (SESANS) provides accurate information about particle composition, including the degree of solvent penetration into the polymer brush grafted on to the PMMA spheres to prevent aggregation. It confirms for particles, between 85 nm and 150 nm in radius that inter-particle correlations closely follow the Percus–Yevick hard-sphere model when the colloidal volume-fraction is between 30% and 50% provided the volume-fraction is used as a fitted parameter. No particle aggregation occurs in these systems. When small amounts of polystyrene are added as a depletant to a concentrated suspension of PMMA particles, short-range clustering of the particles occurs and there is an increase in the frequency of near-neighbor contacts. Within a small range of depletant concentration, near-neighbor correlations saturate and large aggregates with power law density correlations are formed. SESANS clearly separates the short- and long-range correlations and shows that, in this case, the power-law correlations are visible for inter-particle distances larger than roughly two particle diameters. In some cases, aggregate sizes are within our measurement window, which can extend out to 16 microns in favorable cases. We discuss the advantages of SESANS for measurements of the structure of concentrated colloidal systems and conclude that the method offers several important advantages.

Introduction

The hard-sphere system provides a simple and convenient framework for describing correlations between colloidal particles. In this model, spherical particles do not interact when their separation is larger than the particle diameter and they experience infinite repulsion when they are in contact. The structure, dynamics and phase behavior of the hard-sphere system have been thoroughly investigated using various approaches, including liquid theories, computer simulations, and experimental studies.[1–3] Results from these approaches have shown considerable agreement and have led to the hard-sphere system becoming a popular reference model.

One way in which the effective interaction between hard spheres can be modified in a controlled way makes use of depletion forces that arise when smaller particles are added to a colloidal suspension of large particles. The smaller particle may be compact colloidal particles or extended polymer chains. Maximization of the entropy of the smaller particles leads to an attractive effective potential between the larger particles,[4] the depth and range of which can be tuned by varying the size and concentration of the smaller particles. Colloid–polymer binary mixtures display a rich phase behavior that includes crystal nucleation, a glass transition and gelation and have attracted attention from researchers for several decades.[5–7] Nevertheless, the kinetic evolution of the structure close to the phase transition point, in terms of short- and long-range spatial correlations, is still not clear, nor is its relationship to the strength of the depletion force.

[a]*Center for the Exploration of Energy and Matter, Indiana University, Bloomington, Indiana, USA. E-mail: rpynn@indiana.edu*

[b]*Neutron Scattering Sciences Directorate, Oak Ridge National Laboratory, Oak Ridge, Tennessee, USA*

[c]*School of Physics and Astronomy, University of Edinburgh, Mayfield Road, Edinburgh, Scotland*

[d]*Center for Nanophase Materials Science, Oak Ridge National Laboratory, Oak Ridge, Tennessee, USA*

[e]*Manual Lujan Neutron Scattering Center, Los Alamos National Laboratory, Los Alamos, New Mexico, USA*

[f]*Rutherford Appleton Laboratory, Chilton, Oxfordshire OX11 0QX, UK*

A number of recent studies have challenged several fundamental aspects of the description of hard-sphere systems and colloid–polymer mixtures. Sterically stabilized poly(methyl methacrylate) (PMMA) particles have shown hard-sphere-like behaviors in concentrated colloidal suspension,[8] and are commonly selected as the hard colloids for comparison with theories and simulations. Bryant *et al.* used a surface force apparatus to demonstrate that PMMA colloids stabilized by a brush of short poly(hydroxystearic acid) (PHSA) molecules have very hard interaction potentials when decalin is used as a suspension medium, except perhaps in the case of very small particles.[9] Even so, Royall *et al.* concluded that, especially in the case of larger particles of this type used for confocal microscopy studies, caution was needed in mapping behavior of the colloids to a hard-sphere model. In particular, they argued, the effective volume fraction of colloidal particles is difficult to determine accurately.[10] This may lead to a shift in the phase transition lines not only in the phase diagram of the hard-sphere system, but also for colloid–polymer mixtures. In colloid–polymer mixtures, the depletion force, which has been characterized as a mean field potential using Monte Carlo simulation and self-consistent field theory, is strongly dependent on the size ratio of the depletant and the colloid as well as the volume fraction of the colloids.[11,12] The accuracy of the determination of the volume fraction and, furthermore, the determination of the strength and range of the depletion attractive potential, is critical to understanding the behavior of colloid–polymer mixtures.

A number of recent papers have used confocal microscopy to track the positions of colloidal particles in a suspension and to infer the radial distribution function. At low densities, this method provides an accurate way to determine inter-particle interactions. Even at high concentrations, where many body effects are important, obtaining the interaction potential from a real-space correlation function may be a less poorly conditioned problem than the inversion of the structure factor, $S(q)$, measured in traditional radiation scattering experiments. As Royall *et al.* point out,[10] residual attraction or softness of the inter-particle potential shows up much more clearly in the real-space, radial distribution function than in the structure factor.

Spin-echo small-angle neutron scattering (SESANS), is a novel scattering technique which measures a projection of the real-space Debye correlation function, instead of the Fourier transform of this quantity that is generally obtained from conventional small-angle neutron scattering (SANS).[13] SESANS has a number of advantages for the study of dense colloids. It overcomes the issue of multiple scattering in dense colloidal suspensions which hinders the application of dynamic light scattering, microscopy and SANS in surveying concentrated dispersions close to their phase transition points.[14] Even in the presence of strong multiple scattering, SESANS gives a two-particle correlation function without the need for any corrections. The technique can also measure correlations over a wider range of length scales than SANS making it suitable for measuring length scales from a few tens of nm to a few microns. Perhaps most important for the study presented here, SESANS yields a correlation function in real space, intrinsically separating long- and short-range correlations that are mixed with each other in the usual scattering function measured by SANS. The method provides a statistical average over the whole sample and can easily access a range of different particle sizes, including particles that are significantly smaller than those used for microscopy. These advantages of SESANS make it a promising tool to explore inter-particle correlations in hard-sphere systems with and without added depletants.

In this paper, we use SESANS to study the development of the inter-particle correlations in sterically stabilized PMMA suspensions with depletion forces induced by polystyrene (PS) polymers of two different molecular weights. We find that the short- and long-range correlations behave quite differently when the concentrated dispersion approaches the phase transition line. Furthermore, SESANS permits us to measure the total scattering of the system, which cannot be accessed reliably using conventional SANS. This quantity provides accurate information about the geometry of individual PMMA particles as well as the degree of solvent penetration into the polymer brush that is grafted to the particle surface to prevent aggregation.

Materials and methods

The experiments reported here were done with three different colloidal samples of PMMA. In each case, the nominally spherical PMMA particle cores were prepared according to a published procedure[15] and coated with a PHSA polymer brush to prevent aggregation. This involved utilizing a single-stage process to produce the particles which were coated with a prefabricated, sterically stabilizing, polymer brush of poly-12-hydroxystearic acid. After manufacture the particles were cleaned of any excess monomer and stabilizer by centrifugation and redispersion in clean solvent; a routine that also allowed the solvent to be changed if required. This process was repeated ten times to make sure that all the unreacted material and any unwanted solvent had been removed from the system. For most of the neutron experiments, we used decalin as a solvent because it has an optical refractive index that is close to that of PMMA, thereby minimizing the van der Waals (vdW) interactions between spheres. Indeed, Ohtsuka *et al.*[16] estimated using Monte Carlo techniques that residual vdW attraction in this case was about $(0.75 \pm 0.25)\ kT$. Our solvent usually consisted of a mixture of protonated and deuterated decalin (usually in a 60 : 40 ratio), chosen to optimize the neutron scattering contrast between PMMA and the solvent. In this solvent the gravitational height (*i.e.* the height over which the gravitational potential of a particle in the solvent equals its thermal energy) for PMMA particles is of order 1 mm. Since the height of our neutron beam is $\sim$4 mm, we do not expect significant sedimentation during the course of a roughly 1 hour measurement. Furthermore, gravity will have no effect on the inter-particles correlations since these involve a length scale many orders of magnitude smaller. The short PHSA brush on the PMMA surface is intended to prevent the PMMA particles approaching one another too closely and experiencing residual vdW attraction. The overlap of extended brushes on neighboring particles costs significant energy so that the hard-sphere radius of the particles

should be close to the radius of the PMMA core plus the length of the PHSA chains. The three PMMA samples that we have used all made use of the same stock of PHSA, so we might expect the brush thickness to be the similar for each sample. In practice, variations of the grafting density of the PHSA may have some effect on the actual thickness of the layer. Nominally, the radii of our particles were 100 nm, 130 nm and 150 nm as determined by DLS experiments with dilute samples of PMMA spheres suspended in protonated decalin. In each case, samples for neutron scattering were prepared by adding freeze-dried, PHSA-coated PMMA particles to a mixed protonated and deuterated decalin solvent. The mass of solid material added to achieve a given volume fraction of PMMA was calculated using the bulk PMMA density and assuming each particle consisted only of PMMA. Since the PHSA is less than 5% of the total dry weight of the particles, the discrepancy is small. Because of extension of the PHSA chains in the solvent, however, the actual volume fraction may differ from the nominal value calculated from material densities, as we discuss later in the paper.

The neutron scattering length density (SLD) of the decalin solvent and the PMMA are calculated using known values for the material density and the neutron scattering lengths of the constituent nuclei. We expect the solvent to penetrate into the PHSA brush to some extent so there may be a radial variation of the SLD in this region if the extent of penetration depends on the distance from the surface of the PMMA core. However, to model the neutron scattering we have assumed that the SLD is an unknown constant throughout the brush region, but that the degree of solvent penetration may vary from sample to sample. Since the SLD of PHSA is close to zero while that of the solvent is quite large (2.88×10^{-4} nm^{-2} for a 60 : 40 mixture of protonated and deuterated decalin) our experiments are quite sensitive to the degree of solvent penetration into the brush.

We used polystyrene (PS) with two different molecular weights (110 kDa and 900 kDa) or small PMMA particles as depletants in our experiments. Our principal solvent, decalin, is approximately a theta solvent for PS,[23] so we expect radii of gyration of approximately 9.3 nm for 110 kDa polystyrene and approximately 26.5 nm for 900 kDa PS.[17] The small spheres had a nominal total radius of 30 nm and were also coated with the same PHSA brush as the large spheres. Some experiments were performed using dodecane as a solvent. Dodecane is a poor solvent for PS so the radii of gyration of the PS molecules are much less than in the case of the decalin solvent. At the concentrations we used (<1.0% PS by weight), polystyrene depletants caused no observable change in correlations between PMMA particles when dodecane was used a solvent because PS was in a collapsed state.

Spin Echo Small Angle Neutron Scattering (SESANS)

SESANS is a technique that uses Larmor precession of neutron spins to encode the scattering angle of each neutron that is deflected by a sample. The technique has been described in detail in several papers.[13,14,18] In this section, we summarize some of the key results needed to analyze our data, using a notation familiar to practitioners of traditional Small Angle Neutron Scattering (SANS). Some of the equations we present are identical to those given by Andersson *et al.*[18] in their discussion of the analysis of SESANS. We establish a connection between these results and those used in the analysis of traditional SANS data. There are some subtleties because symbols used (and carefully defined) by Andersson *et al.* do not always have the meaning expected by SANS practitioners.

The quantity measured in a SESANS experiment is the average polarization of a neutron beam that has passed through the sample to be studied. For non-magnetic samples, the unscattered part of the beam retains the polarization, P_0, of the incident neutrons, while the part of the beam that is scattered by the sample is depolarized somewhat. The extent to which the scattered beam is depolarized depends on the neutron scattering cross section of the sample and on the magnitude of a parameter called the spin echo length, z, which is essentially the correlation distance probed in the sample. In practice, z is controlled by the neutron wavelength and by various distances and magnetic fields that define the SESANS instrument.[14] The average polarization, $P(z)$, of the neutron beam that has passed through the sample is given by:

$$\frac{P(z)}{P_0(z)} = \exp\{\Sigma_t[G(z) - 1]\} \tag{1}$$

where Σ_t is the fraction of the neutron beam that is scattered *at least once* by a sample of thickness t. The correlation function $G(z)$ is related to a Debye-type autocorrelation function, $\gamma(r)$, defined as:

$$\gamma(r) = \frac{\int_V \Delta\rho(\vec{r'})\Delta\rho(\vec{r'} + \vec{r})\mathrm{d}\vec{r'}}{\int_V \Delta\rho(\vec{r'})\Delta\rho(\vec{r'})\mathrm{d}\vec{r'}} \tag{2}$$

here $\Delta\rho(\vec{r})$ is the difference between the neutron scattering-length density (SLD) averaged over the whole sample and the scattering-length density at position $\vec{r}$. The integrals in eqn (2) are taken over the volume, V, of the sample. The vector sign on the left side of eqn (2) is omitted because we assume that the sample is isotropic on average. In terms of $\gamma(r)$, the correlation function $G(z)$ which appears in eqn (1) may be expressed as[18]

$$G(z) = \frac{2}{\xi}\int_z^\infty \frac{\gamma(r)r}{(r^2 - z^2)^{\frac{1}{2}}}\mathrm{d}r \tag{3}$$

Thus, $G(z)$ is a projection of the autocorrelation function, $\gamma(r)$, onto the z axis in exactly the same way that a conventional radiograph is a projection of the density of an object on to a plane. The transform defined in eqn (3) is called an Abel transform. The normalization constant ξ in eqn (3) defines the correlation length for the scattering sample and is defined by:[18]

$$\xi = 2\int_0^\infty \gamma(r)\mathrm{d}r \tag{4}$$

One may think of ξ, roughly, as a measure of the average size of a region of correlated scattering-length density in the sample.

As we will see below, it is also intimately related to the total neutron scattering cross section of the sample.

For a system composed of hard, uniform spheres suspended in a uniform carrier medium, both $\gamma(r)$ and $G(z)$ are independent of the actual SLDs of the particles and carrier because of the normalization in eqn (2): the dependence on the SLDs of both the numerator and the denominator in eqn (2) are the same. For a more complex system, such as the core–shell particles we investigate, this is not true. In that case, both $\gamma(r)$ and $G(z)$ depend to some extent on the ratios between the SLDs of all of the components of the scattering system.

To understand this point, it is useful to relate $G(z)$ to the neutron scattering cross section per unit volume of sample, $\mathrm{d}\sigma/\mathrm{d}\Omega$ that is measured in a conventional Small Angle Neutron Scattering (SANS) experiment. The relationship, for a sample that scatters isotropically is:[18]

$$G(z) = \frac{\lambda^2 t}{2\pi\Sigma_t}\int_0^\infty J_0(qz)\frac{\mathrm{d}\sigma}{\mathrm{d}\Omega}(q)q\mathrm{d}q \tag{5}$$

where λ is the neutron wavelength and $J_0(x)$ the zeroth order cylindrical Bessel function. For homogeneous particles of SLD ρ suspended in a fluid of SLD ρ_0, the scattering cross section is usually written as the product of a structure factor, $S(q)$, and the square of a normalized form factor, $F(q)$, *i.e.*

$$\frac{\mathrm{d}\sigma}{\mathrm{d}\Omega}(q) = \frac{N}{V}(\rho-\rho_0)^2 S(q)|F(q)|^2 \tag{6}$$

where N is the total number of particles present in the system. When each particle consists of a core whose SLD is ρ_c surrounded by a shell with an SLD of ρ_s, the expression becomes a little more complex:

$$\frac{\mathrm{d}\sigma}{\mathrm{d}\Omega}(q) = \frac{N}{V}\left[(\rho_c-\rho_0)\left(\frac{R_c}{R}\right)^3 + (\rho_s-\rho_0)\left\{1-\left(\frac{R_c}{R}\right)^3\right\}\right]^2 S(q)|F(q)|^2 \tag{7}$$

where R_c is the radius of the particle core and R is the total particle radius. For both homogenous and core–shell particles, the structure factor, $S(q)$, describes correlations between particles. For hard spheres, the Percus–Yevick approximation allows $S(q)$ to be written in terms of simple analytic functions that involve only the particle radius and the volume fraction, ϕ, of particles in the system.[19] This theory applies both to homogeneous and core–shell particles because the only length scale in the theory is the overall particle radius. For any particle – homogeneous or core–shell – the normalized form factor, $F(q)$, is given by:

$$F(q) = V_p\left(\int_{\text{particle}} \mathrm{e}^{-i\vec{q}\cdot\vec{r}}\Delta\rho_0(\vec{r})\,\vec{\mathrm{d}r}\right)\Big/\left(\int_{\text{particle}}\Delta\rho_0(\vec{r})\vec{\mathrm{d}r}\right) \tag{8}$$

where $\Delta\rho_0(\vec{r})$ is the difference between the SLD at position $\vec{r}$ within the particle and the SLD of the suspending fluid. Notice that the normalized form factor tends to a value equal to the volume of the particle, V_p, as $q \to 0$ but that only in the case of a homogeneous particle is the shape of the form factor completely independent of scattering contrast because $\Delta\rho_0(\vec{r})$ is constant inside the particle in this case, leading to cancellation of the SLD contrast between the numerator and denominator of eqn (8). Eqn (8) implies that the form factors in eqn (6) and (7) have different shapes because the distribution $\Delta\rho_0(\vec{r})$ is different in the two cases.

We have deliberately written the equations above in terms of the structure factor and normalized form factor generally used to interpret experiments using Small Angle Neutron Scattering or SANS. These expressions differ somewhat from those presented by Andersson *et al.*[18] in their description of analysis methods for SESANS. A correspondence between the two notations is easy to establish by noting that the quantity, $I(q)$, used by Andersson *et al.* is related to the scattering cross section per unit volume by the equation:

$$\frac{\mathrm{d}\sigma}{\mathrm{d}\Omega}(q) = \langle\Delta\rho^2\rangle I(q) \tag{9}$$

here, $\langle\Delta\rho^2\rangle$ is the average of the squared scattering contrast, defined by Feigin and Svergun[20] for a system with either two or three scattering components as:

$$\langle\Delta\rho^2\rangle = \sum_{i\neq j}\phi_i\phi_j(\rho_i-\rho_j)^2 \tag{10}$$

where ϕ_i and ρ_i are respectively the volume fraction and SLD of the i'th component (*i.e.* the core, shell or carrier fluid in our case). Combining eqn (6), (9) and (10) for a system of homogeneous particles in a carrier fluid yields:

$$I(Q) = \frac{1}{(1-\phi)V_p}S(q)\left|F(q)^2\right| \tag{11}$$

where $\phi = NV_p/V$ is the volume fraction of the particles. Because the symbol $I(q)$ tends to be used by practitioners of SANS to represent the total cross section rather than the quantity defined carefully by Andersson *et al.*, it is easy to confuse these functions and, for example, to omit the term $(1-\phi)$ in eqn (11). Obviously this leads to incorrect answers. An analogous but more complex expression for $I(q)$ for core–shell particles follows from eqn (7), (9) and (10).

Finally, the total (single) scattering probability, Σ_t, which will turn out to be an important quantity in our data analysis, takes the form:[18]

$$\Sigma_t = \frac{\lambda^2 t}{2\pi}\int_0^\infty \frac{\mathrm{d}\sigma}{\mathrm{d}\Omega}(q)q\mathrm{d}q = \frac{\lambda^2 t}{2\pi}\langle\Delta\rho^2\rangle\int_0^\infty I(q)q\mathrm{d}q = \lambda^2 t\langle\Delta\rho^2\rangle\xi \tag{12}$$

Evidently, the total scattering probability is proportional to the correlation length, ξ, in the sample. The above equations demonstrate that SESANS is sensitive both to correlations of scattering length density within the sample (through the function $G(z)$) and to the total neutron scattering (through the parameter Σ_t).

Measurement of PMMA suspensions

We have carried out a number of SESANS experiments on PMMA samples using instruments located at the Los Alamos Neutron Science Center (LANSCE), at the ISIS facility in the UK and at Technical University of Delft in the Netherlands. Very

similar results are obtained at each facility in spite of the fact that each of them uses a different experimental method to implement SESANS: magnetic Wollaston prisms[20,21] on the Asterix beam line at LANSCE, adiabatic rf flippers on the OFFSPEC instrument at ISIS and inclined, magnetized-foil spin-flippers at Delft. SESANS is a relatively new technique so the fact that results from different facilities overlap for a given sample is an important verification that the technique works as intended.

According to eqn (12), the total coherent neutron scattering from a suspension of particles scales as the neutron wavelength squared and the sample thickness. Thus, according to eqn (1), a plot of $\frac{1}{(\lambda^2 t)} \ln\left[\frac{P(z)}{P_0(z)}\right]$ should reach a constant value at large z because $G(z)$ tends to zero at large z as correlations on longer length scales vanish. The quantity $\frac{1}{(\lambda^2 t)} \ln\left[\frac{P(z)}{P_0(z)}\right]$ is one that we will plot frequently. Unfortunately, SESANS is such a young technique that the quantity does not yet have a name. We propose calling it "the wavelength and sample-thickness normalized SESANS signal" or simply "the normalized SESANS signal" for short and will use this name in the remainder of this paper.

From eqn (1), it follows that $G(z)$ and Σ_t can be determined independently from measurements of $P(z)$ and $P_0(z)$ by writing

$$G(z) = 1 - \frac{\ln\left[\frac{P(z)}{P_0(z)}\right]}{\ln\left[\frac{P(\infty)}{P_0(\infty)}\right]} \quad (13)$$

and

$$\ln\left[\frac{P(\infty)}{P_0(\infty)}\right] = -\Sigma_t \quad (14)$$

For homogeneous particles, $G(z)$ does not depend on the SLD of either particle or the solvent because the same multiplicative factors involving the SLDs appear in the numerator and denominator of eqn (2). Thus, for homogeneous particles, the correlation function and the total scattering cross section can be analyzed separately. In that case, $G(z)$ provides information *only* about inter-particle correlations while the total scattering, Σ_t, is related *only* to the SLD contrast and the average correlation distance in the sample. For homogeneous particles, the analysis of $G(z)$ and the total scattering can thus be separated. However, for more complex scattering systems, such as the core–shell particles we examine here, the separation is not possible and one has to fit the full z-dependent, normalized, SESANS signal, $\frac{1}{(\lambda^2 t)} \ln\left[\frac{P(z)}{P_0(z)}\right]$. As shown in Fig. 1, the correlation function calculated using eqn (5) and (6) and the Percus–Yevick form for $S(q)$ for hard spheres does a very good job of describing our data for PMMA spheres of different radii when the nominal volume fraction of particles is 40%. The fits also provide information about the core and total particle radii and the SLD of the PHSA brush.

Using the core and total radii of the particles obtained from the fits, we can calculate the average mass density of the particles and hence a better estimate of their volume fraction. The volume fraction calculated in this way turns out to be between 45% and 49% for our samples instead of the nominal value of 40%. Fitting the data to the PY theory using this volume fraction does not significantly alter the values displayed in Table 1 (*i.e.* the new values are within the errors quoted in the table) but it does result in fits with slightly higher values for chi-squared (for example, 2 rather than 0.7 for the 150 nm particles) that differ from the data in a systematic way. These systematic differences are similar, though less pronounced than those shown in Fig. 3 and may be a sign of slight softness of the inter-particle potential or of residual attraction.

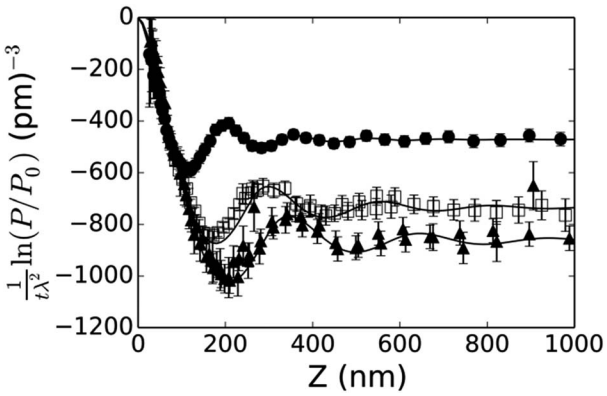

Fig. 1 The normalized SESANS signal plotted as a function of spin echo length for three colloidal suspensions of PMMA particles all with nominal volume fractions of 40%. In each case the solvent was a 60 : 40 mixture of protonated and deuterated decalin. Closed circles: 100 nm nominal-radius particles measured on OFFSPEC at ISIS; open squares: 130 nm nominal-radius particles measured on Asterix at LANSCE; closed triangles: 150 nm nominal-radius particles measured on OFFSPEC. Lines are fits to the Percus–Yevick model described in the text.

Our results indicate that the solvent occupies more than 85% of the volume of the PHSA brush in our particles (*cf.* Table 1). This is consistent with the fact that PHSA made up 5% of the total weight of the particulate material (PMMA + PHSA) during synthesis. If none of the PHSA was removed by washing after particle synthesis, the volume occupied by PHSA can be obtained using the bulk density of PHSA and the fitted dimensions of the composite PMMA/PHSA particles. This calculation indicates that only about 15% of the corona would be expected to be PHSA with the bulk of this region taken up by the decalin solvent, consistent with the results we obtain. We find that the PHSA layer is thinnest for the smallest of our particles. When the particles are synthesized, the mass ratio of

Table 1 Colloidal parameters deduced from the fits shown in Fig. 1

Nominal total radius (nm)	Fitted total radius (nm)	Fitted brush length (nm)	Fraction of brush occupied by solvent
100	89 ± 2	13 ± 2	0.95 ± 0.05
130	132 ± 3	19 ± 2	0.89 ± 0.05
150	150 ± 4	19 ± 3	0.88 ± 0.05

PHSA to PMMA is the same for each sample so the grafting density could be higher for larger particles, making an extended brush more likely. The overall particles sizes from our fits are similar to those obtained from DLS. The largest difference occurs for the smallest particles where our results give a total radius of 89 nm compared to 100 nm reported by DLS. We regard this agreement as reasonable given that DLS measures a hydrodynamic radius and SESANS measures the hard-core radius that enters the PY theory. The thickness of the PHSA layer is within the range of values (10–20 nm) anticipated from chemical knowledge of the sample preparation procedures.

The fits to the PMMA data illustrate a difference between SESANS and SANS that may be important in other investigations. With SANS it is often necessary to make measurements on dilute samples to determine the form factor $F(q)$ and hence the particle geometry. More concentrated samples are then measured to study inter-particle correlations. With SESANS, both particle geometry and inter-particle correlations can be often obtained directly from data on a single, concentrated sample. This could be important if, for example, the particles were to have different degrees of deformability in dilute and concentrated suspensions. Another difference between SESANS and SANS for these investigations is illustrated by comparing our results to those obtained many years ago by the Ottewill group.[8] In order to examine concentrated dispersions with SANS, this group was obliged to use a low scattering contrast between particles and solvent to avoid problems with multiple neutron scattering. This led to SLDs of the PHSA and the solvent being almost equal and obscured the fact that solvent penetrates significantly into the PHSA brush. SESANS is inherently insensitive to multiple neutron scattering so strongly contrasting components can be used.

In Fig. 2, we plot the normalized SESANS signal at large spin echo lengths $\left(i.e.\ \frac{1}{(\lambda^2 t)}\ln\left[\frac{P(z)}{P_0(z)}\right]\right)$ as a function of the fitted core radii of our PMMA particles and find a straight-line behavior with the best fit line passing very close to the origin. To understand this result, we note that fits to our data have found that the SLD of the PHSA brush region is very close to that of the solvent, so most of the scattering contrast is between the PMMA core and the solvent. Thus, from the neutron perspective, our system looks almost the same as a homogeneous PMMA particle with a radius equal to the fitted core radius in our model. According to eqn (1), (10) and (12), the normalized SESANS signal at large spin echo length should be proportional to $\langle\Delta\rho^2\rangle\xi$, provided the sample thickness is the same for each sample, which it is in our case. Because of the high penetration of the solvent into the PHSA brush, the $\langle\Delta\rho^2\rangle$ defined by eqn (10) is almost the same for each of our samples, so the asymptotic SESANS signal only varies because ξ varies between samples. At low volume fraction, $\xi \rightarrow 3R/2$ for a homogeneous particle but as the volume fraction of particles is increased, inter-particle correlations decrease the value the correlation length. Within the PY approximation, the factor by which ξ is decreased depends only on volume fraction for homogeneous particles as shown by Andersson *et al.*[18] Since all of the samples reported in Fig. 2 had the same volume fraction of colloids, the fact that the data in the figure fall on a straight line through the origin is to be expected, provided that the solvent is the major component in the brush region and the correlations between the particles are governed by a formalism within which correlations depend only on particle volume fraction. Fig. 2 thus provides support for these two conclusions.

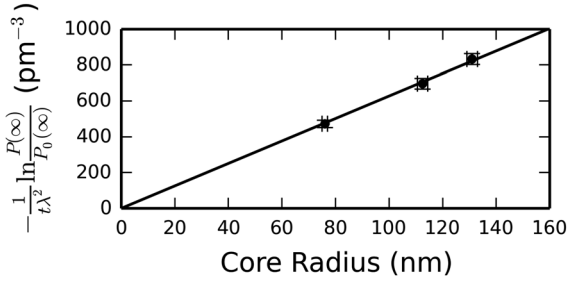

Fig. 2 Plot of the asymptotic SESANS signal *versus* the fitted core radius of PMMA particles in three different suspensions.

Inter-particle correlations in pure PMMA suspensions

Several recent papers[10,16] have noted the difficulty of obtaining reliable information about inter-particle potentials from measurements of $S(q)$ because the problem of inverting $S(q)$ to find the inter-particle potential is ill-conditioned. On the other hand, the traditional pair correlation function, $g(r)$, is quite sensitive to changes in the interaction potential. At low particle density, $g(r)$ is proportional to the logarithm of the interaction potential and so mimics the potential directly. At higher particle concentrations, no such straightforward relationship exists but $g(r)$ still depends sensitively on the inter-particle potential. Recent light microscopy experiments with micron-sized particles have shown that the pair correlation function can be used to investigate effective inter-particle potentials.[16] Since SESANS measures an average correlation function in real space, it is natural to ask whether it can provide better information about inter-particle interactions than conventional SANS.

One way to attempt to answer this question is to calculate the changes in $G(z)$ that result from various modifications of the inter-particle potential. Li *et al.*[22] have used integral equation theory, where the structure factor $S(Q)$ is obtained by solving the Ornstein–Zernike equation and a closure equation, to show that for concentrated dispersions, the correlation function, $G(z)$, for particles with short-range attractions has a shallower first dip than that of a hard sphere model. Their results for 40% volume fraction and short-range potentials of depths of a few kT are shown in Fig. 3. The PY hard-sphere model fits our data very well. A change in the first dip of $G(z)$ that resulted from an attraction of 2 kT would be outside the error bars of our data so we conclude that, even at these high volume fractions, any residual, very-short-range attraction must be smaller than this. It is worth noting that a similar form for $G(z)$, with a shallow first dip, was also found by Kruglov *et al.*[24] in their Monte Carlo calculations of charged colloids with short-range attractions, so integral equation theory

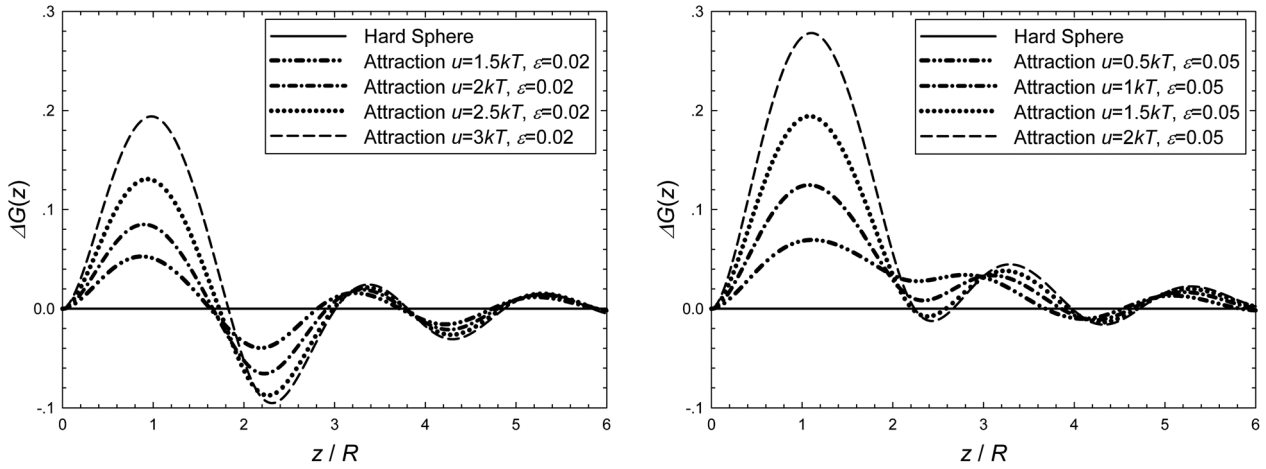

Fig. 3 The difference between the correlation functions, $G(z)$, calculated for particles with a short-range attractive interaction and for hard spheres. The attractive potential is a square well of depth u and width εR where R is the particle radius. The calculation is for a colloid with a 40% volume fraction of homogeneous particles, and is taken from ref. 22.

and Monte Carlo both predict similar qualitative effects on $G(z)$ when short-range inter-particle forces are present.

The overall model for the particles that emerges from our data is of PMMA cores, coated by a polymer brush of PHSA into which the decalin solvent penetrates strongly. Because of entropic effects, the PHSA brush effectively prevents particles penetrating one another, yielding correlations that closely follow the Percus–Yevick solution for hard spheres, although the volume fraction of colloid which gives the best fit is smaller than the volume fraction deduced from the particle size data. Any residual short-range attraction between particles, even for concentrated dispersions, is less than 2 kT. The constancy of the normalized SESANS signal at large values of z, demonstrated for each of our samples in Fig. 1 is clear evidence that correlations have vanished at large particle separations and that there is no aggregation of particles in our PMMA samples.

The effect of short-range inter-particle correlations on $G(z)$

Before turning to results obtained when the effective inter-particle interaction is tuned using depletion forces, it is useful to consider the effects that inter-particle correlations are expected to have on $G(z)$. One of the most intuitively obvious ways to describe correlations in a fluid is through the radial distribution function $g(r)$, which gives the probability, per unit sample volume, of finding a particle with its center a distance r away from another particle. The radial distribution function is directly related to the structure factor $S(q)$ introduced above through the well-known equation:

$$S(q) = 1 + \frac{4\pi}{q}\int_0^\infty \{g(r) - N/V\}\,\sin(qr)r\mathrm{d}r \qquad (15)$$

Combining eqn (5), (6), (8) and (15) allows us to calculate $G(z)$ from any given form of $g(r)$. To develop a more intuitive feeling for $G(z)$, it is useful to calculate the change in $G(z)$ for particular changes in $g(r)$. Because of the structure of the equations, the resulting changes in $G(z)$ will depend to some extent on the form of $g(r)$ before the perturbation is added, but it turns out that this dependence is quite weak. The simplest calculation starts with the form of $g(r)$ appropriate at very low volume fraction where $g(r)$ vanishes for r less than the particle diameter and is unity elsewhere. Suppose we add to this radial distribution function a narrow peak at a particle separation equal to the

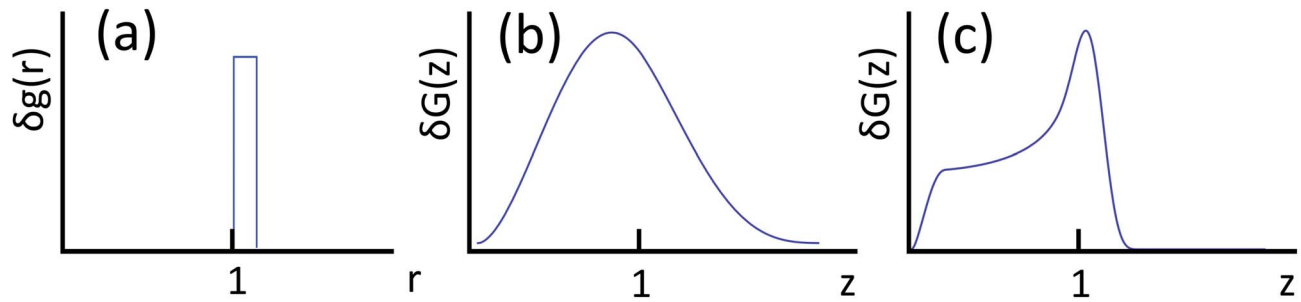

Fig. 4 The effect of short range correlations on $G(z)$. (a) The change in the radial distribution function, $g(r)$, used in the calculations described in the text; (b) the corresponding change in $G(z)$ for homogeneous particles, and (c) the corresponding change in $G(z)$ for a particle whose core, of diameter 1/10 of that of the full particle, is the only part of the particle that scatters neutrons. The abscissa is measured in units of the particle diameter.

particle diameter as shown in Fig. 4a. This added peak represents an increase in the probability that particles are in contact *i.e.* an increase in the number of particles in the first-neighbor shell in an ergodic fluid. If we assume that the particles are homogeneous, the resulting change in $G(z)$ takes the form shown in Fig. 4b. The change is restricted to small values of z, peaking at a value of z close to the particle diameter. The change in $G(z)$ is localized even though it extends over a larger range of inter-particle distances than the change in $g(r)$. This spread turns out to be a result of the particle form factor, as we can easily demonstrate by recalculating the change in $G(z)$ for a core–shell particle in which the core is one tenth of the total particle diameter and in which the shell that has no scattering contrast with the solvent. Using the same perturbation to $g(r)$ depicted in part (a) of Fig. 4, the change in $G(z)$ now resembles quite strongly the change in $g(r)$ which caused it, as shown in part (c) of the figure.

The calculation described above, in which a small perturbation is added to $g(r)$, can easily be repeated with an unperturbed radial distribution function that corresponds to the PY solution for concentrated hard spheres. In this case, using a 40% volume fraction and a homogeneous particle, the change in $G(z)$ resulting from the perturbation to $g(r)$ shown in Fig. 4a peaks at a value of z close to 0.6 times the particle diameter *i.e.* at a smaller value of z than for the case of a dilute colloid. Indeed the change in $G(z)$ in this case is very similar to the curves shown in Fig. 3, except that there are no changes in $G(z)$ for z greater than about 1.5 particles diameters.

A clear conclusion from these calculations is that the SESANS correlation function really does give local information in real space: if we see a change in $G(z)$ that is restricted to a range of z values less than about 1.5 times the particle diameter, we can be sure that it is only nearest neighbor correlations that are changing. Changes in $G(z)$ such as those shown in Fig. 3 and 4, cause changes in $S(q)$ over a large range of q values. To calculate the changes, we carry out a calculation very similar to that described above for the radial distribution function. We start with $G(z)$ for the PY model (using homogeneous spheres and a 40% volume fraction for convenience) and add a Gaussian function as a perturbation that mimics the short-range peak in Fig. 3. We then use the inverse of eqn (5) to calculate the total q-dependent scattering that would be observed in a conventional SANS experiment. Fig. 5 shows a comparison of the scattering obtained with and without the short-range perturbation to $G(z)$. It is clear that the largest change in the scattering occurs at small values of q. Often changes in scattering at low q are blamed on long-range effects such as aggregation, based on the notion that changes at small q must reflect changes in real space at large inter-particle separations because of the Fourier transform relationship between $S(q)$ and $g(r)$. No such confusion is possible in SESANS measurements because the technique presents the correlations in real space and, as we have pointed out above, the constancy of the normalized signal at large z shown in Fig. 1 explicitly precludes the existence of aggregation in our PMMA samples. Moreover, the simplified calculation in Fig. 5 explicitly shows that it is not straightforward to identify the range of correlations responsible for particular changes in $S(q)$.

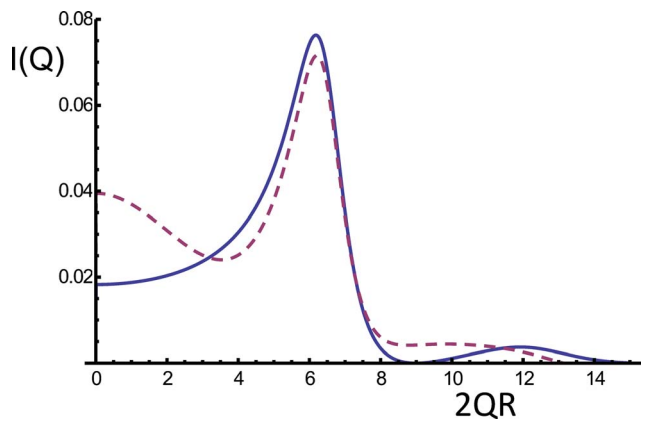

Fig. 5 The effect on $I(Q)$ of adding short-range correlations to $G(z)$. The solid curve is $I(Q)$ for a homogeneous spherical particle of radius R whose inter-particle correlations are calculated from the PY model with a volume fraction of 40%. $G(z)$ is calculated from this curve and then a narrow Gaussian peak of unit height and standard deviation $0.2R$ centered at $1.5R$ is added. The inverse transform of $G(z)$ modified in this way yields the dashed curve in the figure.

Mixtures of PMMA spheres plus polystyrene depletants

We have carried out a number of SESANS experiments in which depletants were added to concentrated PMMA dispersions (30% to 50% nominal volume fractions). For most of these experiments we used a 40% volume fraction of PMMA colloids in decalin and the depletants were small quantities of polystyrene of molecular weight 110 kDa or 900 kDa. The picture that emerges from these experiments is that small amounts of depletant (less than about 0.4% by weight) generally cause changes *only* in the short-range correlations between particles. These changes are restricted to the nearest and perhaps next-nearest particle neighbors only, as demonstrated by parts (a), (b), (c) and (f) of Fig. 6. The measured change in $G(z)$ due to the addition of small amounts of depletant appears to increase with the amount of depletant. This change is of short-range and vanishes, within error, for any value of z greater than about 1.5 particle diameters. The effect of the molecular weight of the depletant molecules is in the direction we would expect: when a similar weight percentage of lower molecular weight depletant is added, the increase in the number of depletant molecules increases the attractive potential induced between PMMA particles (*cf.* Fig. 6b and c).

When 0.5% by weight of depletant is added, the picture revealed by the SESANS measurements changes dramatically. The magnitude of the peak in the normalized SESANS signal at short-range increases somewhat and a long-range power-law tail appears (*cf.* Fig. 6d). The range of the power-law correlations (*i.e.* the value of z beyond which the normalized SESANS signal is constant) varies from sample to sample indicating the development of clusters or aggregates of different sizes. We have

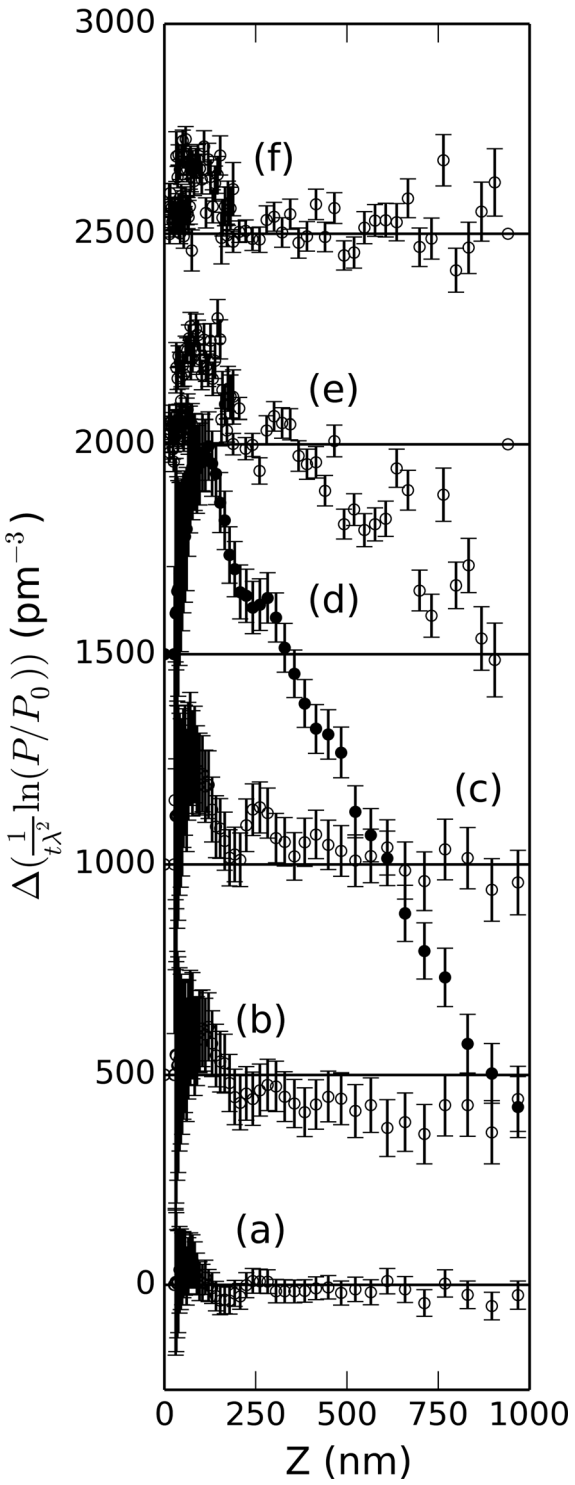

Fig. 6 The difference between SESANS signals with and without a given mass fraction of polystyrene. The PMMA sample comprised 40% (nominal) volume fraction of 100 nm nominal-radius PMMA particles in decalin. The samples with depletants had: (a) 0.2% 900 kDa molecular weight polystyrene; (b) 0.3% 900 kDa polystyrene; (c) 0.3% 110 kDa polystyrene; (d) 0.5% 900 kDa polystyrene; (e) 0.2% 900 kDa polystyrene; (f) 0.3% 110 kDa polystyrene. Data displayed in panels (a) through (d) were measured on OFFSPEC at ISIS while panels (e) and (f) were measured using ASTERIX at LANSCE. Individual data sets have been offset by 500 pm^{-3} for clarity.

observed mean aggregate sizes ranging from ~5 microns to beyond 16 microns (the limit for the SESANS apparatus at Delft; data not shown). Sometimes, samples with less than 0.5% polystyrene also show power law correlations after they have been left standing for some time, as shown in Fig. 6e, although these correlations can be removed easily by sonication. Thus, except perhaps for very small amounts of added depletant, the structures we observe cannot be described by a model in which particle separation is maintained by Brownian motion. At the volume fraction we have probed (nominally 40%), moderate amounts of depletant cause PMMA particles to jam together and to form a gel with long-range power law correlations. Even the short-range effects seen in panels (a)–(c) and (f) of Fig. 6 may represent significant local jamming of particles so that the measured correlation functions cannot be used to extract inter-particle potentials.

To understand better the implications of the difference plots in Fig. 6, we consider a model in which the Debye correlation function can be written as the sum of two parts which we refer to as long-range (LR) and short-range (SR), although we admit the possibility that the two functions may overlap in some region of inter-particle distances. If the Debye correlation function can be written as the sum of two functions so, according to eqn (3), can $G(z)$. Then, using eqn (1) and (12) we may write:

$$\left[\frac{1}{\lambda^2 t}\ln(P/P_0)\right] = \langle\Delta\rho\rangle^2\phi(1-\phi)\left[\xi_{SR}G_{SR}(z) + \xi_{LR}G_{LR}(z) - \xi_{SR} - \xi_{LR}\right] \quad (16)$$

where $G_{SR}(z)$ and ξ_{SR} are obtained from eqn (3) and (4) using the short-range part of the Debye correlation function and the long-range components are defined in a similar way. There are no long-range correlations in the pure PMMA suspension (*cf.* Fig. 1) so $G_{LR}(z) = 0$ in this case and difference between the normalized SESANS signals with and without added depletant takes the form:

$$\Delta\left[\frac{1}{\lambda^2 t}\ln\left(\frac{P}{P_0}\right)\right] = \langle\Delta\rho\rangle^2\phi(1-\phi)\left[\xi_{SR}\Delta G_{SR}(z) + \xi_{LR}\Delta G_{LR}(z) - \xi_{LR}\right] \quad (17)$$

In eqn (17), $\Delta G_{LR}(z)$ represents long-range correlations that may develop when depletant is added and $\Delta G_{SR}(z)$ is the change in the short-range correlations caused by those depletants. The equation is written under the assumption that the short-range correlation length does not change significantly when depletants are added, a condition that is easily verified using the results plotted in Fig. 6. As Fig. 6 shows, when only small amounts of depletant are added, no long range correlations develop (*i.e.* $G_{LR}(z) = 0$), and $\Delta G_{SR}(z)$ appears as a small peak centered around a value of z close to the particle radius. We know from Fig. 4 that such a peak in $\Delta G_{SR}(z)$ implies an increase in the number of nearest neighbor particles due to crowding of the PMMA colloids by the polystyrene depletants. This short-range peak is observed for all levels of added depletant shown in Fig. 6. There is some weak evidence in the data of an increase in

the number of second neighbors but the statistics are not good enough to make strong assertions on this score. When sufficient depletant is added (greater than about 0.5% according to Fig. 6), the correlation function always develops a long-range, power-law tail. However, there is no evidence that the power-law correlations have any effect on the short-range correlations *i.e.* the two functions do not seem to overlap. If the power-law correlations extended down to $z = 0$ when depletants were added the overall shape of the difference curves in Fig. 6 would change at small z when long-range power law correlations were established: indeed the small-z peak would be expected to change to a dip. Thus, the data tell us that the power-law correlations extend down to distances on the order of two particle diameters and then a separate functional form describes short-range effects. Short-range correlations with and without depletants are very similar although the frequency of near neighbor contacts increases as depletants are added, perhaps indicating the formation of more and more small clusters of jammed particles. Eventually, these clusters assemble into large aggregates. The transition from a fluid of small clusters to one with aggregates occurs over a small range of depletant concentration and seems to be history dependent (*cf.* parts (a) and (e) of Fig. 6). This picture is quite similar to the one revealed by optical microscopy in dilute samples of PMMA colloid when larger (2.25 micron diameter) beads are used.[16]

Conclusions

We have shown that SESANS provides an accurate measure of the solvent penetration into the PHSA brush used to stabilize suspensions of PMMA particles. In principle, this information could also be determined using conventional SANS. However, doing so requires measuring with confidence the absolute value of the scattering from a dilute sample at very small values of momentum transfer Q. A simple calculation shows that there is very little difference in the actual scattering obtained with different amounts of solvent penetration for momentum transfers Q greater than about $2\pi/d$. For our particles, this means that a conventional SANS experiment would have to be able to make measurements with high absolute accuracy for $Q \sim 0.001$ Å^{-1} and below. While certainly not impossible, such an absolute measurement would require excellent calibration of the SANS instrument as well as confidence that no aggregation of particles had occurred within the sample. On the other hand, SESANS measures the total scattering accurately, without the need for independent calibration. Furthermore, measurement out to high spin echo lengths allows the experimenter to determine unambiguously whether or not aggregation has occurred. Finally, the SESANS experiment can be carried out using the same concentrated dispersion that is used to measure inter-particle correlations, obviating the need to assume that particles have the same geometry in both dilute and concentrated dispersions.

Our results show that there is significant solvent penetration into the PHSA brush for all particle sizes but that the amount of solvent penetration decreases as the particle size increases. This makes sense given that the same ratios of PHSA to PMMA were used in each of the preparations, leading probably to a higher grafting density for larger particles. The higher grafting density also seems to result in a greater stretching of the PHSA brush for larger particles and hence a slightly greater brush thickness.

Our SESANS experiments with concentrated dispersions of PMMA show, as has been previously reported based on other types of measurement, that the Percus–Yevick, hard-core model describes accurately the correlations between PMMA particles stabilized with a PHSA brush. The volume fraction of the colloids used to fit the PY theory to the data is, however, lower than we would estimate based on the fitted particle dimensions and the weight of the particles used to make the dispersions. An advantage of SESANS for this type of measurement is that the technique can be used with concentrated, strongly scattering samples without fear that multiple scattering of radiation (neutrons in our case) will affect the results. Using the results of calculations based on integral equation theory, we are able to assert that any attractive, short-range potential between the PMMA spheres must have a magnitude of less than 2 kT. An attractive potential larger than this would lead to a correlation function that falls outside the statistical error bars of our measurement. It would not be difficult to reduce this limit by making a longer measurement with higher statistical accuracy.

Sufficiently small amounts of polystyrene added as a depletant to concentrated PMMA suspensions cause *only* an increase in the frequency of nearest neighbors around each PMMA particle. When the amount of depletant is increased beyond a threshold, the increase in the frequency of nearest neighbors saturates and long-range power law correlations appear. The size of the aggregates formed varies from sample to sample. Power law correlations extend down to particle separations around two particle diameters. Given that we occasionally observe long-range correlations to occur in samples with very small amounts of added depletant, it seems plausible that the increase in the frequency of near-neighbor contacts in this case could be due, at least in part, to non-ergodic clustering of particles.

Acknowledgements

We thank Chris Duif of the Interfaculty Reactor Institute in Delft for carrying out several SESANS measurements on our samples and Wim Bouwman of the same institute for helpful comments on the manuscript. This work was supported by the U.S. Department of Energy through its Office of Basic Energy Sciences, Division of Material Science and Engineering (grant no. DE-FG02-09ER46279). ABS is partially funded by the UK Engineering and Physical Sciences Research Council grant EP/J007404/1. A portion of this research was conducted at the Center for Nanophase Materials Sciences, which is sponsored at Oak Ridge National Laboratory by Office of Basic Energy Sciences, U.S. Department of Energy. We thank the ISIS facility in the UK and the Los Alamos Neutron Science Center (LANSCE) for the award of beam time. Los Alamos National Laboratory is operated by Los Alamos National Security LLC under DOE Contract DE-AC52-06NA25396.

Notes and references

1 M. Wertheim, *Phys. Rev. Lett.*, 1963, **10**, 321.
2 A. Trokhymchuk, I. Nezbeda, J. Jirsak and D. Henderson, *J. Chem. Phys.*, 2005, **123**, 024501.
3 M. A. Rutgers, J. H. Dunsmuir, J.-Z. Xue, W. B. Russel and P. M. Chaikin, *Phys. Rev. B: Condens. Matter Mater. Phys.*, 1996, **53**, 5043.
4 H. N. W. Lekkerkerker and R. Tuinier, *Colloids and the Depletion Interaction*, Springer, Dordrecht, Heidelberg, London, New York, 2011.
5 P. N. Pusey and W. van Megen, *Nature*, 1986, **320**, 340.
6 W. C. K. Poon, *Curr. Opin. Colloid Interface Sci.*, 1998, **3**, 593.
7 K. Kroy, M. E. Cates and W. C. K. Poon, *Phys. Rev. Lett.*, 2004, **92**, 148302.
8 I. Markovie, R. H. Ottewill, S. M. Underwood and Th. F. Tadros, *Langmuir*, 1986, **2**, 625.
9 G. Bryant, S. R. Williams, L. Qian, I. K. Snook, E. Perez and F. Pincet, *Phys. Rev. E: Stat., Nonlinear, Soft Matter Phys.*, 2002, **66**, 060501.
10 C. P. Royall, W. C. K. Poon and E. R. Weeks, *Soft Matter*, 2013, **9**, 17.
11 M. Doxastakis, Y.-L. Chen and J. J. de Pablo, *J. Chem. Phys.*, 2005, **123**, 034901.
12 A. I. Chervanyov and G. Heinrich, *Phys. Rev. E: Stat., Nonlinear, Soft Matter Phys.*, 2012, **86**, 021801.
13 R. Pynn, in *Neutron Spin Echo*, ed. F. Mezei, Springer-Verlag, Berlin, 1980.
14 M. T. Rekveldt, *Nucl. Instrum. Methods Phys. Res., Sect. A*, 1996, **114**, 366.
15 L. Antl, J. W. Goodwin, R. D. Hill, R. H. Ottewill, S. M. Owens, S. Papworth and J. A. Waters, *Colloids Surf.*, 1986, **17**, 67.
16 T. Ohtsuka, C. P. Royall and H. Tanaka, *Europhys. Lett.*, 2008, **84**, 46002.
17 W. C. K. Poon, *J. Phys.: Condens. Matter*, 2002, **14**, R859.
18 R. Andersson, L. F. van Heijkamp, I. M. de Schepper and W. G. Bouwman, *J. Appl. Crystallogr.*, 2008, **41**, 868.
19 N. W. Ashcroft and J. Lekner, *Phys. Rev.*, 1966, **145**, 83.
20 L. A. Feigin and D. I. Svergun, *Structure Analysis by Small Angle X-ray and Neutron Scattering*, Plenum, New York, 1987.
21 R. Pynn, M. R. Fitzsimmons, W. T. Lee, P. Stonaha, V. R. Shah, A. L. Washington, B. J. Kirby, C. F. Majkrzak and B. B. Maranville, *Physica B*, 2008, **404**, 2582.
22 X. Li, C.-Y. Shew, Y. Liu, R. Pynn, E. Liu, K. W. Herwig, G. S. Smith, J. Lee Robertson and W.-R. Chen, *J. Chem. Phys.*, 2010, **132**, 174509.
23 H. L. Wagner, *J. Phys. Chem. Ref. Data*, 1985, **14**(4), 1101.
24 T. V. Kruglov, W. G. Bouwman, I. M. de Schepper and T. M. Rekveldt, *Physica B*, 2005, **356**, 218.